ELSEVIER

Polymer 40 (1999) 871–885

polymer

Mixture design approaches to IPDI–H_6XDI–XDI ternary diisocyanate-based waterborne polyurethanes

Chien-Hsin Yang[a,*], Huey-Jia Yang[a], Ten-Chin Wen[b], Ming-Sieng Wu[b], Jian-Sheng Chang[b]

[a]*Department of Environmental and Chemical Engineering, Kung Shan Institute of Technology, Tainan, Taiwan*
[b]*Department of Environmental and Chemical Engineering, National Cheng Kung University, Tainan 701, Taiwan*

Received 11 December 1997; accepted 13 April 1998

Abstract

A systematic modelling analysis for polyaddition of poly(butylene glycol adipate) [PBA] to isophorone diisocyanate (IPDI), xylene diisocyanate (XDI) and hydrogenated xylene diisocyanate (H_6XDI) ternary diisocyanate-based waterborne polyurethane (WPU) synthesized by a modified acetone process was performed. Using a mixture of experimental designs, empirical models are fitted and plotted as contour diagrams, which facilitate revealing the synergistic/antagonistic effects between the mixed diisocyanates. The results indicate that each component demonstrates different performances in either binary (IPDI–XDI, XDI–H_6XDI and IPDI–H_6XDI) or ternary (IPDI–XDI–H_6XDI) systems with the IPDI-based WPU, which possesses the highest tensile strength. The largest ultimate elongation occurs at $\frac{1}{3}$IPDI/$\frac{1}{3}$$H_6$XDI/$\frac{1}{3}$ XDI ternary diisocyanate-mixed WPU. Particle size analysis shows that the larger particles are obtained in the dispersion of IPDI–XDI binary WPU. Differential scanning calorimetry (DSC) results show that PBA polyol and its converted WPU show doublet melting behaviour. A plot of $1/T_m^L$ (lower melting temperature) against $-\ln X_{IPDI}$ (mole fraction of IPDI in mixed diisocyanates) is approximately linear, indicating that the hard segments are randomly distributed along the molecular chain. Wide angle X-ray diffraction (XRD) and polarized microscopy (POM) on these WPU films were also examined.

Keywords: Waterborne polyurethane; Mixture design; Ternary diisocyanate

1. Introduction

Polyurethane (PU) is a segmented polymer comprising alternating sequences of soft segments and hard segments which constitute a unique microphase separation structure. In the case of a high degree of phase separation, hard segments tend to generate glassy on crystalline regions, and randomly arranged soft segments form amorphous regions [1]. For PU, the characteristic of crystalline and non-crystalline coexistence provides a significant effect upon the mechanical properties [2].

A waterborne polyurethane (WPU) dispersion is a binary colloidal system in which PU particles are dispersed in a continuous water phase. Particle size is variable from approximately 1 to 5000 nm and has a direct impact on PU dispersion stability in which the dispersion with large average particle sizes ($>$ 1000 nm) is generally unstable with respect to sedimentation. Smaller average particle sizes ($<$ 200 nm) are sought after, since such dispersions are storage stable and possess a high surface energy, resulting in a strong driving force for film formation [3]. Generally, aqueous PU dispersions are prepared by incorporating hydrophilic groups into the main polymer chains [4,5]. Three types of hydrophilic groups, cations, anions and zwitterions, are usually employed, and form cationomers [6–9], anionomers [10–14] and zwitterionomers [15], respectively.

Polyurethane ionomers (PUIs) are PU polymer chains bonding ionic groups, which are usually prepared by reaction of a NCO- terminated PU prepolymer with a chain extender containing COOH pendent groups, followed by neutralization with base [13,16]. On the other hand, polyurethane ionomers are also prepared by sulfonating the urethane linkage in 1:1 copolymers of diisocyanates and polyols [17]. A considerable research effort has been made to understand the microstructure of PUI, which strongly affects their physical properties [18,19]. Up to now, a variety of techniques has been used to study PUI morphology; especially, small angle X-ray scattering (SAXS) [20] analyses have revealed that the ionizable groups of the MDI-based PUIs are regularly spaced. The SAXS data for these ionomers show both the usual ionomer peak and a prominent shoulder at higher angle, reflecting an ordering of the ionic microdomains.

* Corresponding author.

0032-3861/98/$ - see front matter
PII S0032-3861(98)00300-0

Various processes have been developed for the preparation of WPU [1–11,13,16]. A modified acetone process has been successfully utilized in our previous papers [21,22] that deals with the viscosity build-up of the extremely fast NCO-NH chain extension reaction. A suitable amount of acetone (auxiliary solvent) together with powerful agitation is employed in controlling viscosity during the dispersal step, while a blocked diamine (i.e. acetimine) is used as a latent chain extender in order to control the NCO-NH reaction. Dimethylolpropionic acid (DMPA) is utilized as the ionic component in the preparation of NCO- terminated PU prepolymer containing COOH groups. Pendent COOH groups are subsequently neutralized with triethylamine (TEA). The resulting prepolymer is then extended through reaction with an ethylene-diamine derivative bearing sulfonate groups, as shown in Scheme 1. Carboxylate and sulfonate anions chemically bound to the PU backbone, which remain fixed to the PU particles surface, whereas the counter-cations (i.e. Na and TEA) are attracted by anions (COO^- and SO_3^-) and migrate into the aqueous phase. This phenomenon exists in the equilibrium state.

Recently, a polyester-urethane was synthesized by the reaction of 2,4-tolylene diisocyanate (TDI) with poly(butylene glycol adipate) (PBA) [23]. The results of atomic force

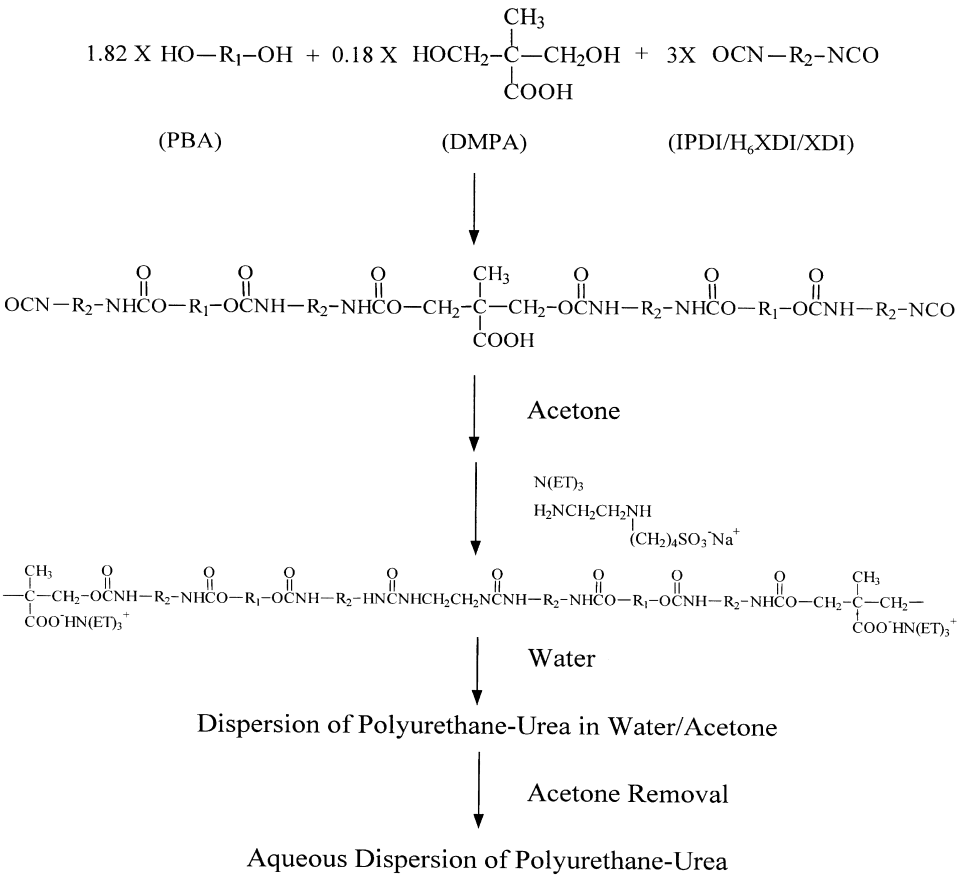

where:

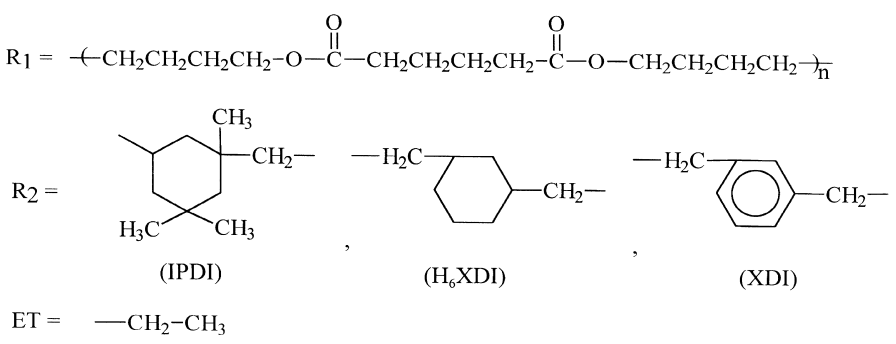

Scheme 1. Preparation process for waterborne polyurethane dispersion.

microscopy proved that the surface of this PU film appeared as a spherulitic structure with a varied diameter and vertical height. On the other hand, the comparison between hydrogenated diphenylmethane diisocyanate (H_{12}MDI) and isophorone diisocyanate (IPDI) on the dispersion properties of PU anionomers was studied [24]. Polyurethanes from H_{12}MDI showed coarser dispersion and better tensile properties over those from IPDI. In practice, IPDI, H_6XDI and XDI are usually selected as main raw materials for PU series in adhesives or coatings. The use of IPDI (or H_6XDI)-based PU in the formulations of adhesive, although the weather resistance of this product is very excellent, would mean that the film of such an adhesive would exhibit some defects due to lower peel strength and lower water resistance. Accordingly, to promote the resulting product performance of adhesive, it is expected that IPDI (or H_6XDI) would be mixed with other better physical properties of diisocyanate to tailor-make a modified IPDI (or H_6XDI)-based PU adhesive possessing better strength. In the case of this work, XDI is naturally a candidate for its excellent property and chemical similarity. Unfortunately, these previous experiments only focused on a single component of diisocyanate, thereby severely lacking the scope of a binary or ternary diisocyanate system study. For the ternary diisocyanate-based WPU dispersion, however, no efficient experimental strategy exists that explores the full properties against compositional relations. In order to gain an overall view, this paper statistically examines the properties of various ternary diisocyanate-based WPU dispersions by the mixture design method [25]. This experimental strategy effectively models the dependence of resulting solution viscosity, particle size, film properties, respectively, on IPDI–H_6XDI–XDI ternary diisocyanate compositions.

Mixture design strategy is based on statistical analysis, where a limited number of experiments is used to study the multicomponent system. The experimental region can be represented by a regular simplex, and since the sum of the component proportions is unity, this region is a triangle. The experimental region is explored at a point of composition corresponding to an ordered arrangement. The mixture design method assumes that the properties of the WPU dispersion are a function of its component (IPDI, H_6XDI, XDI) compositions. This relationship can be expressed as

$$\eta = f(x_1, x_2, x_3)$$

where the variable x_i represents the molar proportions of IPDI (x_1), H_6XDI (x_2) and XDI (x_3), respectively, in the diisocyanate composition of the WPU dispersion.

In this study, a forward stepwise regression procedure [26] was employed to achieve a statistically significant regression equation. The regression model was then plotted as a property-against-composition contour diagram on a computer program, which facilitated straightforward interpretations of the properties of binary and ternary diisocyanate systems. Ideally, this work will shed an insight into the dependence of WPU dispersion properties of diisocyanate composition.

2. Experimental section

2.1. Preparation of WPU dispersion

The raw materials employed in this study are listed in Table 1. Poly(butylene glycol adipate) were dried and degassed *in vacuo* at 70°C for two days. Acetone was dried by distillation over P_2O_5 and stored over 3 Å molecular sieves before use. All other chemicals were used without further treatment.

An outline of the modified acetone process used in this study for preparation of WPU dispersion is shown in Scheme 1. In this study, a mixture design was utilized in planning the diisocyanates (IPDI–H_6XDI–XDI) in the appropriate molar ratios (refer to Table 2). A total of 16 experiments was performed under the optimum conditions obtained in our previous work [21].

The segmented prepolymer (PBA–DMPA–PU) used in this study was synthesized by a one-step addition reaction. To a 1000 ml four-necked round-bottomed flask complete with an anchor-propeller stirrer 7 cm in length and 2 cm in width, a nitrogen inlet and outlet, and a thermometer, a solution of PBA (100 g, 0.1 mol) and DMPA/NMP (0.134 g/2.866 g) was charged under a nitrogen gas atmosphere, and a diisocyanate mixture of IPDI–H_6XDI–XDI (0.165 mol) was then added slowly over a period of 1 h

Table 1
Raw materials

Designation	Chemical identification	Suppliers
PBA	Poly(butylene glycol adipate) $M_w = 2000$	Nan Pau Co.
IPDI	Isophorone diisocyanate	Wako Chemical Co.
H_6XDI	Hydrogenated xylene diisocyanate	Wako Chemical Co.
XDI	Xylene diisocyanate	Wako Chemical Co.
DMPA	Dimethylol propionic acid	Tokyo Kasei Co.
NMP	N-methyl-2-pyrrolidinone	Aldrich Chemical Co.
EDA	Ethylenediamine	Merck Chemical Co.
BS	Butane sultone	Aldrich Chemical Co.
NaOH	Sodium hydroxide	Wako Chemical Co.
TEA	Triethylamine	Merck Chemical Co.

Table 2
Design matrix and experimental results of IPDI–H_6XDI–XDI ternary diisocyanate-based waterborne polyurethane

Run	Diisocyanate compositions			Appearance	Viscosity at 25°C (Pa·s)	Dispersion				Film properties	
	x_1(IPDI)	x_2(H_6XDI)	x_3(XDI)			Hydraulic particle size (nm)	$T_m^{L\,a}$	$T_m^{U\,b}$	γ^c	Ultimate elongation (%)	Tensile stress (MPa)
1	1	0	0	milky white	0.0105	152.3	36.40	45.24	2.40	10	17.38
2	0	1	0	milky white	0.0110	319.7	40.80	47.35	2.11	15	15.46
3	0	0	1	milky white	1.1250	82.5	41.63	48.49	0.93	10	16.12
4	1/3	1/3	1/3	milky white	0.0965	147.9	38.90	45.99	3.10	60	12.00
5	1/2	1/2	0	milky white	0.0520	305.3	37.96	46.58	1.22	55	13.11
6	0	1/2	1/2	milky white	1.1750	233.7	42.15	49.07	2.10	40	12.00
7	1/2	0	1/2	milky white	0.0304	619.5	37.10	46.93	1.43	42	13.82
8	2/3	1/6	1/6	milky white	0.0223	492.7	38.87	46.59	1.66	55	14.30
9	1/6	2/3	1/6	milky white	0.0555	140.2	40.42	47.58	1.06	58	12.87
10	1/6	1/6	2/3	milky white	0.0841	140.2	39.89	46.50	2.78	50	10.78
11	3/4	1/4	0	milky white	0.0151	404.5	36.39	45.19	2.11	45	15.11
12	1/4	3/4	0	milky white	0.0725	248.8	40.65	47.70	2.44	65	12.00
13	1/4	0	3/4	milky white	0.1026	92.4	35.24	44.19	2.63	50	14.50
14	3/4	0	1/4	milky white	0.0260	683.5	39.19	46.78	3.01	90	10.38
15	0	3/4	1/4	milky white	0.8980	254	40.16	46.99	1.01	70	11.48
16	0	1/4	3/4	milky white	0.9800	97.8	41.82	47.52	1.80	80	11.91

[a]The melting temperature of the lower peak.
[b]The melting temperature of the upper peak.

under gentle stirring (200 rpm). The mixture was heated at 80°C until the theoretical NCO content of the prepolymer was reached, as determined by the di-n-butylamine titration method [27]. The final NCO-terminated PU prepolymer solutions were adjusted to acetone/PU ratios of 3.65 through addition of a suitable amount of acetone. Typical molecular masses of PU prepolymers are listed in Table 3.

Triethylamine (1 g), a neutralizing agent, and an ethylenediamine-based chain extender bearing sulfonate groups in aqueous solution (5.3 g; see preparation of chain extender) were added immediately to the freshly prepared NCO-terminated PU prepolymer solution. The resulting mixture was then heated at a phase-inversion temperature of 50°C for 10 min, yielding PU anionomers in acetone.

Doubly distilled water (*ca*. 140 g) was added to neutralized PU anionomer solutions at agitation rate and water addition rate of 500 rpm and 2.0 ml/min, respectively. An aqueous dispersion of *ca*. 40 wt% solids was obtained upon removal of acetone by rotary vacuum evaporation.

2.2. Preparation of the chain extender

Ethylenediamine (6.0 g, 0.1 mol) was added dropwise to a solution of butane sultone (13.6 g, 0.1 mol) and H_2O (25 g). The resulting mixture was heated at 70–80°C for 30 min and then cooled to room temperature, after which NaOH (4.0 g, 0.1 mol) was added. The aqueous solution of chain extender possesses a pale yellow colour, normal boiling point of 105.5°C and specific gravity of 1.14. Water was evaporized out of the reaction mixture to yield a pale yellow powdery compound: mp:35.5–36.0°C. ^{1}H n.m.r. (D_2O): δ 3.98–4.20 (q, 4H, -$(CH_2)_2$-), 4.90–5.38 (m, 8H, -$(CH_2)_4$-), 7.14 (s, 1H, -NH-), 7.22 (s, 2H, -NH_2). *FT*i.r.: Wavenumbers (cm^{-1}): 3445 (N-H stretching, H-bonded), 2948 (C-H asymmetric stretching, in CH_2), 2876 (C-H symmetric stretching, in CH_2), 1654 (N-H bending), 1459, 1408 (C-H symmetric bending, in CH_2), 1352 (S(=O)$_2$ asymmetric stretching, in SO_3^-), 1186 (S(=O)$_2$ symmetric stretching, in SO_3^-), 1044 (C-N stretching), 793–609 overlap region: 793–677 (N-H wagging), 793 (strong S-O-C stretching), 677–609 (broad N-H out of plane bend).

2.3. Measurements

The MWD and average molecular weight of the PU prepolymer were determined by GPC (Shimatsu R-7A data module, LC-10AS pump). The separation columns were 2-linear columns in series. The flow rate for THF was 1 ml/min at 40°C using polystyrene standards. Viscosity was determined at 25°C using a Brookfield digital viscometer (Model DV-II). Dispersion particle size was measured by an Otsuka, Model LPA 3000/3100 laser scattering spectrophotometer. This procedure involved diluting a few drops of the dispersion in distilled water

Table 3
Molecular mass distribution of PU prepolymers

Run	Diisocyanate compositions			$\bar{M}_{FUNCn}$	$\bar{M}_{FUNCw}$	$\bar{M}_w/\bar{M}_n$
	x_1(IDPI)	x_2(H_6XDI)	x_3(XDI)			
1	1	0	0	16 567	27 328	1.65
2	0	1	0	26 536	92 479	3.49
3	0	0	1	57 773	178 880	3.10
4	1/3	1/3	1/3	21 675	45 517	2.10

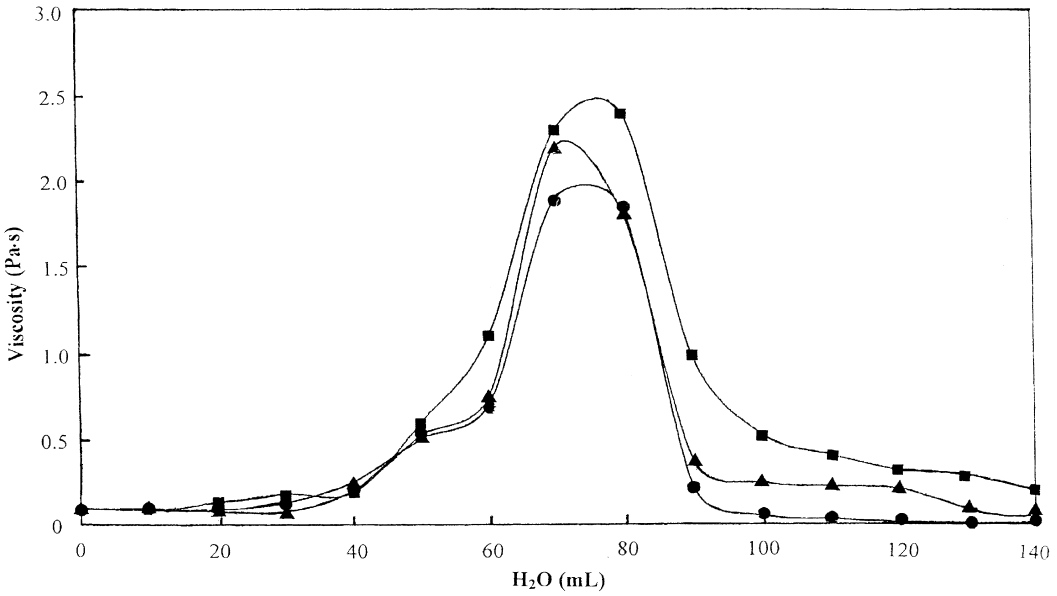

Fig. 1. Viscosity variation of PU solutions during water addition: (●) pure IPDI-based WPU dispersion, (▲) pure H_6XDI-based WPU dispersion and (■) pure XDI-based WPU dispersion, respectively.

prior to spectrophotometric measurement. The results of three runs were averaged in order to obtain the hydraulic-average particle size of the dispersion.

Differential scanning calorimetry (DSC) was carried out over a temperature range from − 60 to 120°C using a Du Pont 910 DSC at a heating rate of 10°C/min. Polarizing optical microscopy of WPU films was performed with a Nikon Optiphof-2POC polarizing microscope (POM) equipped with a Nikon NFX-35 camera. Films were prepared by casting the WPU dispersion on a slide glass, followed by drying at 30°C for 24 h. The remaining moisture was further dried at 30°C, 20 mmHg for 24 h.The X-ray instrument used was a Riguka D/Max II-B with CuKα radiation and a wavelength of 1.542 Å.

Mechanical properties of WPU films under relative humidity of 60% at 25°C were determined using an instron (HT-8335A, Hung-Ta, Taiwan) at a crosshead speed of 50 mm/min. The WPU film specimens were prepared by casting the WPU dispersion on a Teflon plate, followed by drying at 30°C for 24 h. The remaining moisture was further dried at 30°C, 20 mmHg for 24 h.

3. Results and discussion

3.1. Viscosity variation during dispersion

Variations in PUI solution viscosity during water addition to pure IPDI, H_6XDI and XDI-based PU solutions are, respectively, shown in Fig. 1. After the addition of approximately 20 ml of water, PUI solution viscosity drops slightly, with these previously turbid solutions becoming transparent (translucent). The solution viscosity starts to sharply increase following the addition of approximately 60 ml of water, reaching a maximum after the addition of about 75–80 ml of water. Solution viscosity then decreases sharply until a total water addition of approximately 90–95 ml, after which viscosity decreases relatively slowly, reaching a constant value after a total water addition of approximately 120 ml. An increase in viscosity in region I arises from a relative decrease of acetone content in the solution accompanied by chain extension [21], in which polyester segments lose their solvation sheaths and come together forming hydrophobic associates that physically cross-link [16,21]. In region II, further addition of water increases solution turbidity (milky white) and sharply decreases viscosity, suggesting that the hydrophobic associates rearrange forming microspheres during dispersion.

3.2. WPU dispersion viscosity

In order to identify the viscosity characteristics of a WPU dispersion, the resulting dispersion viscosity with all 16 samples was measured. In this study, the dispersion viscosity data are listed together with the design matrix in Table 2. Regression equation coefficients for the viscosity approximation model were calculated from experimental viscosity values in Table 2 with the aid of the appropriate formulas [25], and generated the following equation:

$$\begin{aligned}\nu = {} & 0.045x_2 + 1.104x_3 + 2.160x_2x_3 - 2.358x_1x_3 \\ & + 4820.326x_1x_2x_3 + 2.534x_1x_3(x_1 - x_3) \\ & + 2.385x_2x_3(x_2 - x_3) - 4810.321x_1^2x_2x_3 \\ & - 4848.850x_1x_2^2x_3 - 4837.762x_1x_2x_3^2 \end{aligned} \quad (1)$$

(0.042) (0.057) (0.228) (0.206) (1200.9) (0.459) (0.473) (1201.1) (1201.2) (1201.2)

where x_1, x_2 and x_3, respectively, represent the molar

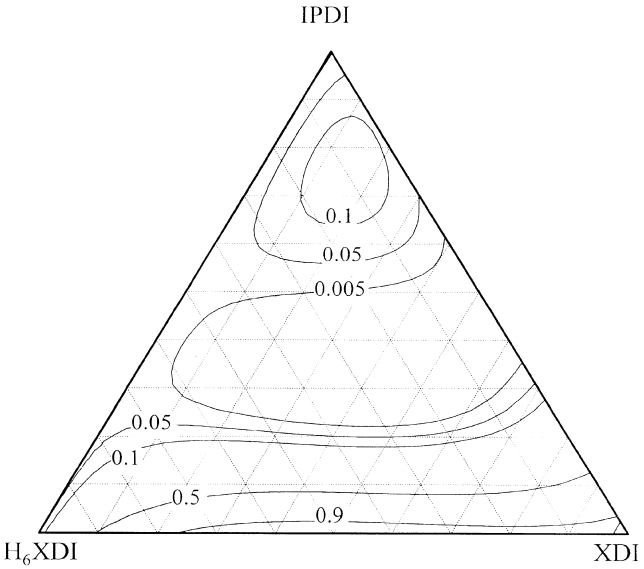

Fig. 2. Contour line plot of WPU dispersion viscosity (Pa·s) against diisocyanate compositions for IPDI–H_6XDI–XDI ternary diisocyanate-based WPU dispersions.

proportions of IPDI, H_6XDI and XDI in the diisocyanate composition. The numbers in parentheses below the coefficients are their standard errors based on error variance estimates (s^2 = mean square of error = 0.0033). The magnitude of the regression equation coefficients compared to their estimated standard errors are used as the basis for judging statistical significance and illustrate the relative effects (synergistic/antagonistic) on viscosity (ν) for the mixed-diisocyanate WPU dispersion.

The analysis of variance of ν is summarized in Table 4. The test statistics, F and R^2_{adj}, are defined as $F = \text{MSR/MSE}$ and $R^2_{adj} = 1 - \text{SSE}/(N-P)/\text{SST}/(N-1)$, where MSR is the mean square of regression obtained by dividing the sum of squares of regression with the degree of freedom. MSE represents the mean square error from the analysis of variance. If the calculated F value is greater than the table $F(p-1,v,1-\alpha)$ value, a 'statistically significant' regression model is obtained, where v is the degree of freedom of error and p is the number of parameters. $F(p-1,v,1-\alpha)$ is the F value at the α probability level. R^2_{adj} is the adjusted correlation coefficient (R^2), with a value close to 1 meaning a perfect fit to the experimental data.

The regression Eq. (1) was used in constructing the contour plots (see Fig. 2) on IPDI–H_6XDI–XDI diisocyanate composition diagram against viscosity for both binary (IPDI–H_6XDI, H_6XDI–XDI and IPDI–H_6XDI) and ternary (IPDI–H_6XDI–XDI) diisocyanate systems. Note that an extreme region with maximum values of ν (*ca.* 0.9 Pa·s) occurs in H_6XDI–XDI binary systems possessing 0–75% H_6XDI. Also note that the value of ν for IPDI–XDI binary systems is of extreme form with *ca.* 0.9 Pa·s maximum values possessing pure XDI, indicating the XDI mixed in the IPDI and H_6XDI polymer chain, leading to higher dispersion viscosity. These results arise from the addition of XDI hydrophobic segments in the polymer chain, leading to the increase in phase separation (physical cross-linking) of the polymer chain which generates a larger viscosity of WPU dispersion.

In the case of H_6XDI–XDI binary systems, the dependence of ν on composition is not of extreme form. Instead, ν is essentially small over the entire compositional range. This result implies the fact that H_6XDI–IPDI-based WPU dispersions are similarly aliphatic segment inside WPU dispersion particles. This aliphatic segment results in the smaller phase separation of the polymer chain, leading to a uniform small viscosity of WPU dispersion particle.

For IPDI–H_6XDI–XDI ternary systems, ν increases with increasing XDI content. An increase in ν follows by an increase in the phase separation of the polymer chain with increasing XDI content, and a decrease in dispersion viscosity with increasing IPDI and H_6XDI contents.

Table 4
Analysis of variance for the fit of ν for IPDI–H_6XDI–XDI ternary diisocyanate-based WPU dispersions

Source	Degrees of freedom	Sum of squares	Mean square	F
Model	10	4.43376	0.44338	134.366
Error	6	0.01980	0.00330	
Total	16	4.45356		

3.3. WPU dispersion particle size

Particle size is determined by dispersion viscosity and stability with respect to sedimentation, while it is predominantly governed by the polarity and orientation of the polymer chain. The particle size was analyzed by using an instrument of dynamic light scattering. A series of typical analysis results is shown in Fig. 3. It is obvious that the IPDI-based WPU dispersion (Fig. 3*a*) corresponds to trimodal distribution of peaks at 20, 120 and 556 nm. The H_6XDI-based WPU dispersion (Fig. 3*b*) generates a bimodal distribution of peaks at 80 and 487 nm. The XDI-based WPU dispersion (Fig. 3*c*) also possesses a bimodal distribution merged with each other at the average value of 83 nm. On the other hand, an examination of Fig. 3*d–f* reveals that the pattern of modal distribution depends significantly on the predominant quantity of diisocyanate in the ternary IPDI–H_6XDI–XDI-mixed WPU dispersions. These results indicate that the modal distribution of particles size increases with decreasing the molecular mass of PU-prepolymer (refer to Table 3), suggesting that the modal distribution of particle size is related to the molecular orientation of diisocyanates and molecular mass of PU-prepolymers.

In order to understand clearly the dependence of particle size on the compositional effects of the mixed diisocyanates, particle size testings with all samples of 16 runs were undertaken.

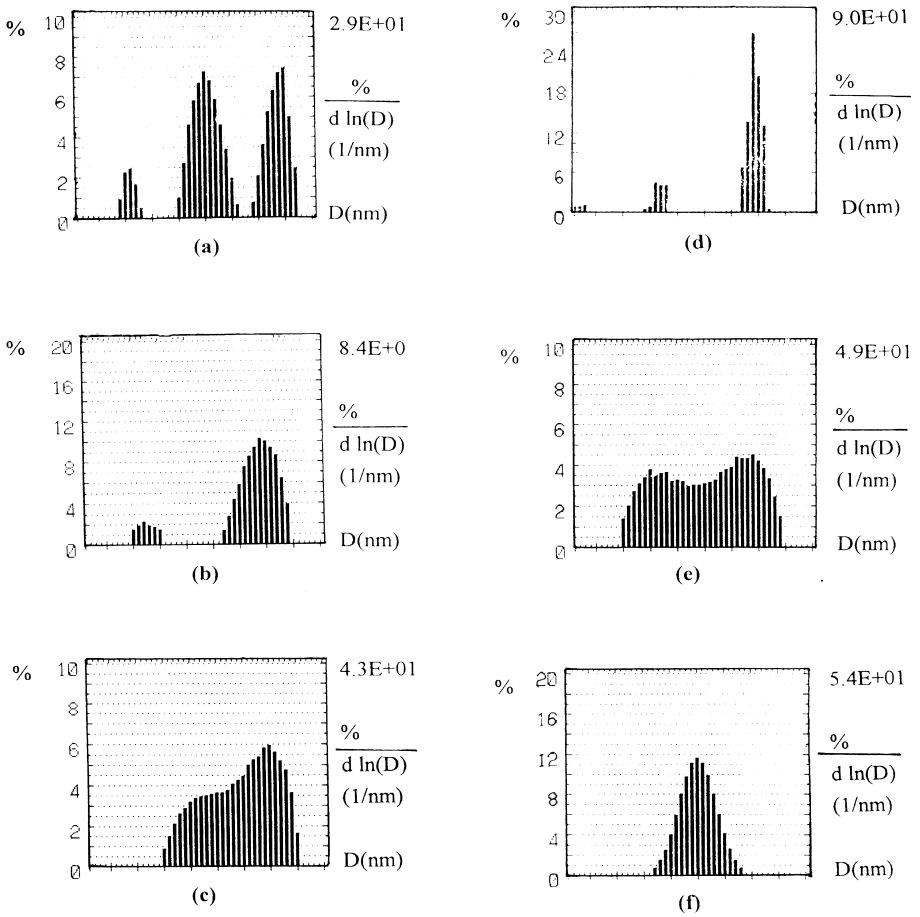

Fig. 3. Particle size distribution of WPU dispersion. The samples are (a) run 1, (b) run 2, (c) run 3, (d) run 8, (e) run 9 and (f) run 10, respectively. The corresponding compositions of runs refer to Table 2.

The regression equation for hydraulic-average particle size (D_p) in Table 2 is of the following form:

$$D_p = 197.04x_1 + 375.56x_2 + 1758.15x_1x_2 + 1011.58x_1x_2(x_1 - x_2) + 2403.91x_1x_3(x_1 - x_3) - 15208.0x_1x_2^2x_3 \quad (2)$$

(49.78) (40.62) (198.03) (458.60) (428.51) (3995.1)

The value of the test statistics, $R^2_{adj}(= 0.9646)$, indicates that the regression model is statistically significant. The contour plot of particle size (D_p) against composition for the IPDI–H_6XDI–XDI ternary diisocyanate system was constructed from Eq. (2) and is shown in Fig. 4.

Note that an extreme region with maximum values of D_p (*ca.* 500 nm) occurs in IPDI–XDI-binary systems possessing 45–90% IPDI composition. This result reflects that IPDI–XDI-mixed PU chain possesses a higher randomness than the pure XDI and IPDI-based PU chains. Also note that the D_p value of an IPDI-based WPU dispersion is close to that of a H_6XDI-based WPU dispersion, but larger than that of a XDI-based WPU dispersion. The latter result is attributable to the fact that finer particle sizes are formed due to less stereohindrance for XDI-based PU-prepolymer chains.

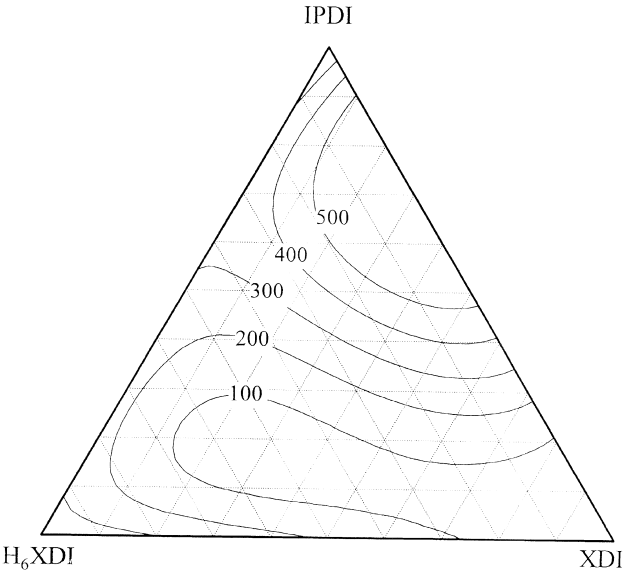

Fig. 4. Contour line plot of WPU dispersion particle size (nm) against diisocyanate compositions for IPDI–H_6XDI–XDI ternary diisocyanate-based WPU dispersions.

A comparison between IPDI–H_6XDI and H_6XDI–XDI binary systems in Fig. 4 reveals that the particle size of the former system is larger than that of the latter. For the IPDI–H_6XDI binary system, D_p decreases with increasing H_6XDI content. One possible explanation for this result is that the addition of H_6XDI leads to a decrease in stereohindrance of polymer chains, resulting in a uniform smaller particle size. For the H_6XDI–XDI binary system, on the other hand, the molecular structures of both H_6XDI and XDI are relatively similar to each other; hence, it would be reasonable to assume that the effect of XDI content on D_p is relatively less significant. These results imply that the molecular similarity is more accessible in H_6XDI–XDI than in IPDI–XDI binary systems, which permit a greater uniformity of molecular orientation.

3.4. Differential scanning calorimetry study

A series of DSC thermograms is shown in Fig. 5. The melting behaviour of the PBA polyol and all WPU samples exhibits two main doublet peaks (located at 35–50°C). For the PBA sample (curve a), the lower peak of the melting doublet dominantly appears at 45.07°C, while the upper peak of the melting doublet appears at 50.75°C.

The behaviour of the main melting doublets for WPU samples, however, was quite different from that for PBA polyol. As PBA polyol was converted into WPU, the relative intensity of the main melting doublets shifted from the lower to upper peak (refer to curves b–e). Semicrystalline polymer, e.g. poly(ethylene terephthalate) [PET] [28–31], has been reported to exhibit closely spaced double-melting endotherms in the major melting region under certain crystallization conditions. Poly(butylene terephthalate) [PBT] was also reported [32–35] to exhibit similar behaviour. Two main mechanisms for the doublet melting behaviour, dual morphology and melting–recrystallization–remelting, have been proposed for the interpretation of such double melting phenomenon. The dual morphology mechanism [33–35] describes that two melting peaks in polymers might be explained by two different spherulite structures. On the other hand, the recrystallization–remelt mechanism proposes that crystallization at lower temperatures generates crystals that may have only a low degree of perfection, and melt and recrystallize to yield crystals of better perfection or greater thickness upon heating scan to a higher temperature [28–31]. Recently, Woo and co-workers [36,37] provided evidence for the postulation of simultaneously existing lamellae of multiple thickness as a result of crystallization and annealing at multiple descending temperature steps. Thus, our DSC results reflect that more polymer chains of PBA polyol crystallize in forming thicker lamellae and less are left to form thinner lamellae.

A closer inspection revealed that the peak area and temperature of these main peaks were related to the kind of diisocyanates in WPU chains. The crystallized WPU exhibited a smaller lower peak compared to the PBA polyol. The upper peak intensity seemed to increase rapidly, and the magnitude of the lower peak decreased relatively for WPU samples. At a sample of IPDI-based WPU (curve b), the progress of crystallization became slower, but the doublet peaks gradually merged with each other. The results suggested that an addition of IPDI content in PU chains resulted in more uniform thickness distribution of the crystals, as evidenced by observation of a sharper and higher

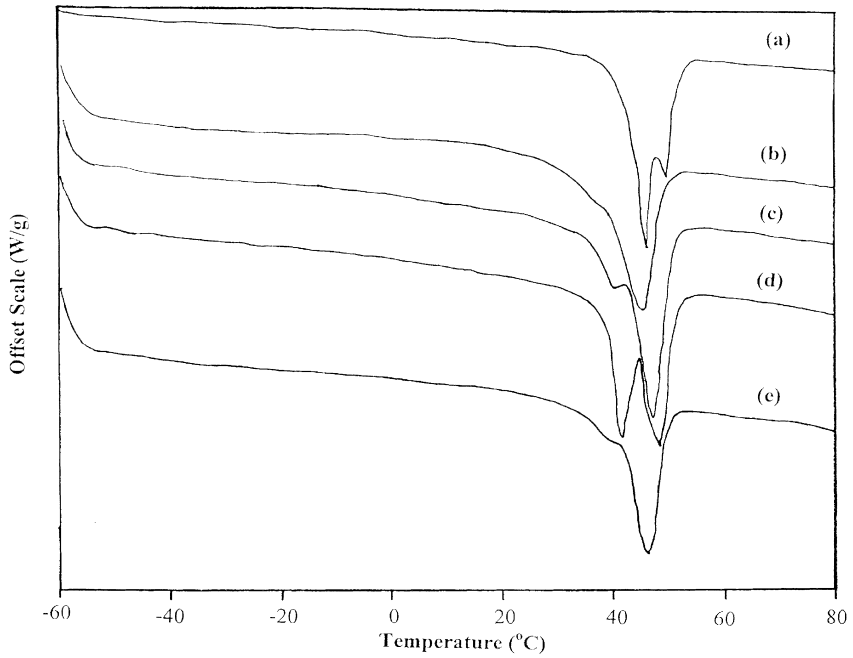

Fig. 5. DSC melting thermograms of WPU films after drying at 30°C for five days. The samples are (a) PBA polyol, (b) pure IPDI-based WPU, (c) pure H_6XDI-based WPU, (d) pure XDI-based WPU and (e) $\frac{1}{3}$IPDI/$\frac{1}{3}H_6$XDI/$\frac{1}{3}$XDI-mixed WPU film, respectively.

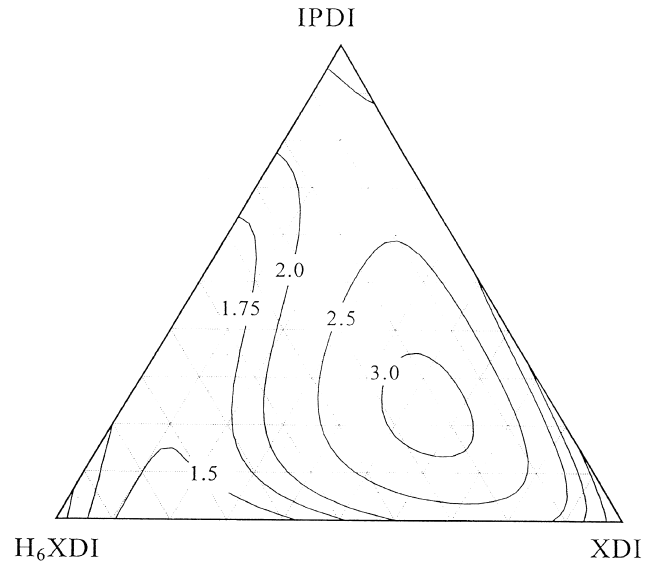

Fig. 6. Contour line plot of relative-magnitude changes of melting enthalpy of lower and upper peaks as a function of diisocyanate compositions for IPDI–H_6XDI–XDI ternary diisocyanate-based WPU films.

melting single peak. There are differences in the melting endotherms observed among these WPU samples. The lower peak (40.78°C) of the melting doublet obviously started to appear in the H_6XDI-based WPU (curve c). More notably, the pronounced lower peak (41.63°C) of the melting doublet was observed in the XDI-based WPU (curve d). That is, the lower peak appearance intensity for these WPU is in the order: XDI > H_6XDI > IPDI-based WPU. A plausible explanation for this result is that more polymer chains of XDI-based WPU crystallize easily in forming thicker lamellae. The lower peak (38.65°C) of the melting doublet was still observed in the ternary diisocyanate-mixed WPU sample (curve e), but the intensity was apparently decreased in comparison with that of XDI-based WPU sample. Similar melting behaviour was also observed in other diisocyanate-mixed WPU samples, whose results are mostly similar to the sample of curve e (Fig. 5) and thus not shown here for brevity.

To quantitatively compare how the relative magnitudes of lower peak versus upper peak changed with the composition variation of diisocyanates, the areas under the doublet peaks were integrated. The ratio $\gamma \equiv$ (melting enthalpy of upper peak)/(melting enthalpy of lower peak) as a function of diisocyanate composition. The results are listed in Table 2 and subjected to regression analysis. This regression analysis generated the following equation:

$$\gamma = 2.54x_1 + 2.09x_2 + 1.39x_3 - 2.72x_1x_2 - 7.13x_2x_3(x_2 - x_3) + 78.75x_1x_2x_3^2 \quad (3)$$

(0.47) (0.51) (0.45) (2.51) (4.92) (42.74)

Note that R^2_{adj} (= 0.9011) indicates a statistically significant regression model. The contour plot of γ against the IPDI–H_6XDI–XDI ternary diisocyanate system composition is shown in Fig. 6. The region of maximum γ value ($\gamma \approx 3$) is observed within the range of 15–30% IPDI/15–30% H_6XDI/45–65%XDI-mixed WPU films, indicating that the melting enthalpy of upper peak increases at the expense of the decrease in that of lower peak. Also note that this γ value decreases with a change in other compositions of diisocyanates. These results suggest that there might be double crystalline lamella entities co-existing with different distributions of lamella thickness, and that the relative magnitudes of these populations of crystals can change as a result of mixed compositions of diisocyanates. It is worthwhile to mention that the γ value of PBA polyol is 0.4167, this value is relatively low in comparison with those corresponding to WPU samples. For PBA polyol, the relative intensity of the main melting doublets shifted from the upper to lower peak. Moreover, the peak temperatures (upper and lower peaks, respectively) of PBA polyol are higher than those of WPU. This result reflects the fact that PBA polyol easily crystallizes in forming thicker lamellae with less left to form thinner lamellae. This is attributable to the PBA polyol being devoid of the addition of other component segments (diisocyanates), leading to a more regular arrangement of molecular chains.

The above results suggested that there were two types of crystals growing in this WPU when crystallized at 30°C for five days. The two different types of crystals are responsible for the doublet peaks in the main melting region. The order of their appearance varied with the crystal sizes. The upper peak always developed first, and the lower peak followed [37]. This fact indicates that the higher-melting crystals develop more quickly, while the lower-melting crystals generally takes a longer time to develop.

In order to evaluate the effect of different diisocyanate compositions on melting temperature, a series of T^U_m (melting temperature of the upper peak) and T^L_m (melting temperature of the lower peak) for WPU samples was directly measured from DSC thermograms, and the results (refer to Table 2) were subjected to regression analysis. This regression analysis generated the following equations:

$$T^L_m = 35.36x_1 + 41.33x_2 + 41.15x_3 \quad (4)$$

(0.56) (0.56) (0.56)

and

$$T^U_m = 44.75x_1 + 47.79x_2 + 47.83x_3 \quad (5)$$

(0.46) (0.46) (0.46)

Note that both R^2_{adj} (= 0.9994 for T^L_m and 0.9997 for T^U_m, respectively) values indicate a statistically significant regression model. The contour plot of T_ms against the IPDI–H_6XDI–XDI ternary diisocyanate composition is, respectively, shown in Figs 7 and 8.

An examination of Fig. 7*a* reveals that various horizontal lines are obtained, and that the T^L_m of WPU linearly moves to

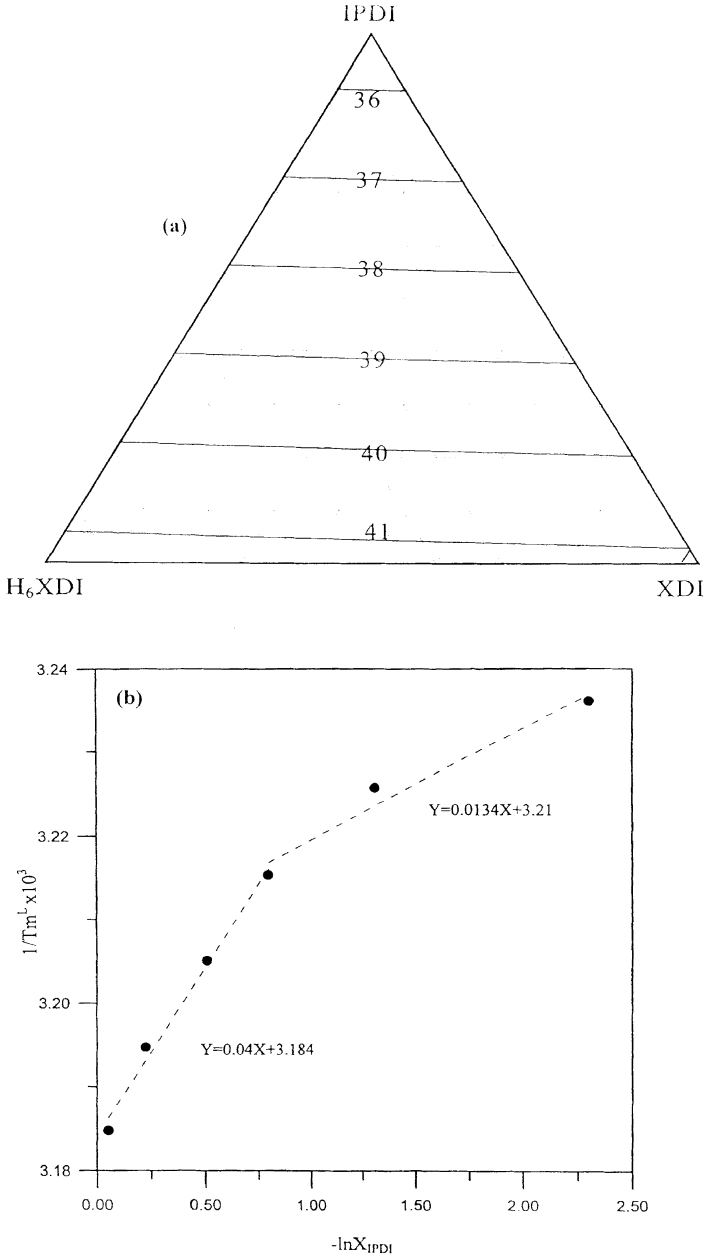

Fig. 7. (a) Contour line plot of T_m^L (lower melting temperature, °C) of WPU films against diisocyanate compositions for IPDI–H_6XDI–XDI ternary diisocyanate-based WPU dispersions. (b) A plot of the reciprocal of the lower melting temperature $1/T_m^L$ against $-\ln X_{IPDI}$ (mole fraction of IPDI in diisocyanate compositions).

lower temperature as the IPDI content increases. The former result is attributable to a similar conformation between H_6XDI and XDI molecules; the latter result implies that melting point depression in random copolymer can be predicted by using a theory developed by Flory [38]. In the present case, the reciprocal of the melting temperature $1/T_m^L$ against $-\ln X_{IPDI}$ is approximately linear (Fig. 7*b*), indicating that the IPDI segments are randomly distributed along the molecular chain of the WPUs used in this study. An extrapolation of $1/T_m^L$ against $-\ln X_{IPDI}$ to $X_{IPDI} = 1$ gives $(1/T_m^L)_{IPDI}$, a reciprocal of the lower melting point of the pure IPDI-based WPU. The value of $(T_m^L)_{IPDI}$ can be estimated at 35.36°C (experimental value is 35.40°C). It is worthwhile to note that there exist two straight lines with different slopes, the critical point at $X_{IPDI} = 0.5$. This result implies that there two different phases occur. One is dominated by IPDI at $X_{IPDI} > 0.5$; the other phase is dominated by both H_6XDI and XDI at $X_{IPDI} < 0.5$. In addition, the T_m^Ls of H_6XDI and XDI-based WPUs are higher that those of IPDI-based WPU. Since the crystal melting points of linear polymers depend on chain flexibility and interchain forces, the equation $T_m^L = \Delta H_m^L/\Delta S_m^L$ provides a correlation between the observed higher peak melting point for XDI and H_6XDI-based WPU. The conformations

of regular rigid chains (

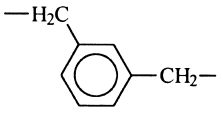

for XDI and

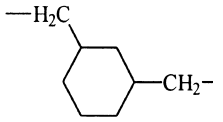

for H_6XDI, respectively) will not be much different in the amorphous state near T_m^L than they are in the crystal lattice. This means that the melting process confers relatively little additional disorder on the system; ΔS_m^L is low and T_m^L is increased accordingly. For example,

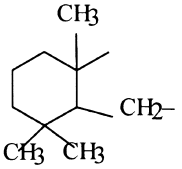

units in IPDI-based WPU, which enlarge the intermolecular distance and offer more free space, make this structure more flexible than XDI/H_6XDI-based WPU, and T_m^L of the former species is only 36.40°C. By contrast, XDI/H_6XDI-based WPU is composed of stiff chains and its crystal melting point is 41.63°C/40.80°C. Because stronger intermolecular forces result in greater ΔH_m^L values and an increase in T_m^L, these XDI/H_6XDI-based WPUs, which are hydrogen bonded, possess higher intermolecular forces with the same degree of polymerization. Thus, the T_m^L of XDI and H_6XDI-based WPUs are higher than those of IPDI-based WPU.

On the other hand, Fig. 8 shows the contour plot of T_m^U against the IPDI–H_6XDI–XDI ternary diisocyanate composition. As seen here, the peak temperatures of the upper peaks are not significantly changed with the variation of diisocyanate compositions. It seems reasonable to assume that the $\Delta H_m^U/\Delta S_m^U$ ratios between these WPU samples are similar with approximately the same T_m^U values.

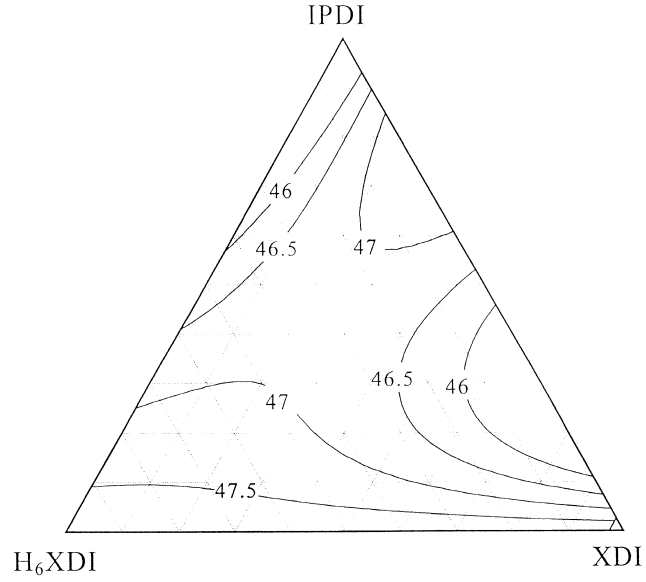

Fig. 8. Contour line plot of T_m^U (upper melting temperature, °C) of WPU films against diisocyanate compositions for IPDI–H_6XDI–XDI ternary diisocyanate-based WPU dispersions.

3.5. Tensile tests

The stress–strain properties of IPDI–H_6XDI–XDI-based WPU films are shown in Fig. 9. It is obvious that the mixed mesophasic hard segment (diisocyanate component) has a profound influence upon the stress at a given strain, probably due to the component effect. The distinct differences in elongation at break between the pure diisocyanate WPU and the mixed diisocyanate WPU can be attributed to the morphological changes in these WPU samples. As compared with pure diisocyanate WPU, the relatively random distribution of the mesophase in mixed diisocyanate WPU leads to low tensile properties and large elongation at break. The superior tensile properties of pure-diisocyanate WPU may result from the presence of a regular lamella or possibly bicontinuous mesophase [39].

In order to evaluate stress performance for overall components of diisocyanates, IPDI–H_6XDI–XDI ternary diisocyanate WPU dispersions were cast to provide films under an air atmosphere (relative humidity of 60%) at 25°C, and the results of their ultimate stress, obtained directly from testing (see Table 2), were subjected to regression analysis. This regression analysis generated the following equation:

$$\tau = 15.54x_1 + 13.67x_2 + 16.07x_3 - 15x_2x_3 - 13.62x_1x_3 \quad (6)$$

(1.17) (1.17) (1.40) (6.05) (6.05)

The value of the test statistics, R_{adj}^2 (= 0.9853), indicates a statistically significant regression model. The contour plot

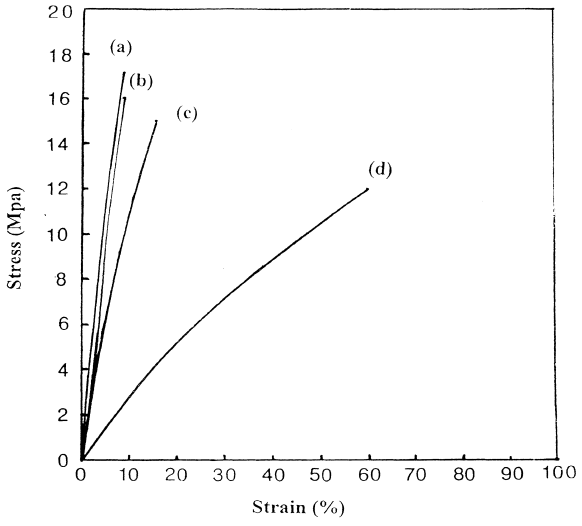

Fig. 9. Tensile test of WPU films. The samples are (a) pure IPDI-based WPU, (b) pure H_6XDI-based WPU, (c) pure XDI-based WPU and (d) $\frac{1}{3}$IPDI/$\frac{1}{3}$$H_6$XDI/$\frac{1}{3}$XDI-mixed WPU dispersions, respectively.

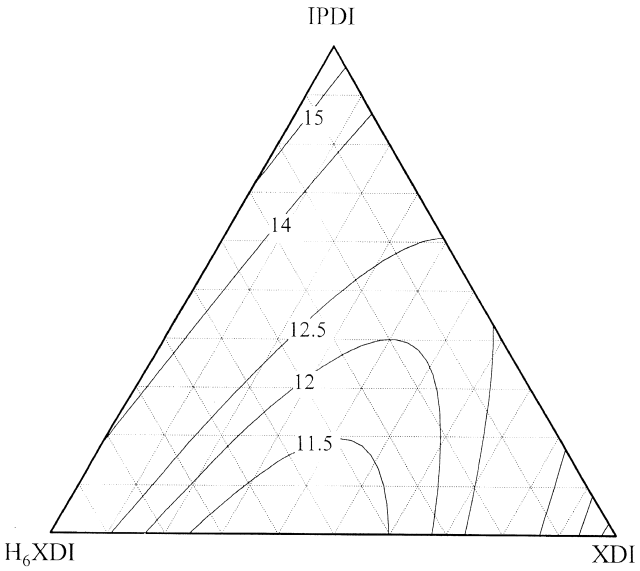

Fig. 10. Contour line plot of film tensile strength of WPU films (MPa) against diisocyanate compositions for IPDI–H_6XDI–XDI ternary diisocyanate-based WPU dispersions.

of stress against the IPDI–H_6XDI–XDI ternary diisocyanate composition is shown in Fig. 10.

An examination of Fig. 10 reveals that a pure IPDI-based WPU film possesses the maximum τ value, and that this value decreases with increasing H_6XDI and XDI contents in either binary (IPDI–H_6XDI and IPDI–XDI) or ternary (IPDI–H_6XDI–XDI) systems. This result suggests the fact that an IPDI-based WPU film possesses a higher stress than the H_6XDI and XDI counterparts. This situation is thought to arise from the fact that IPDI-based WPU possesses a tougher mesophase, which experiences difficulty in inducing chain deformation.

A comparison of the IPDI–H_6XDI and IPDI–XDI binary systems in Fig. 10 reveals that the stress of both systems is approximately close. This result reflects that the chain-deformation effect of these binary diisocyanate-based WPU chains inducing flexibility on the IPDI–H_6XDI system is similar to that on the IPDI–XDI system.

For the H_6XDI–XDI binary system, τ is essentially low over the entire compositional range, indicating that the deformation of molecular chains reducing the stress is approximately the same.

3.6. Ultimate elongation

Ultimate elongation coupled with stress is also an important consideration in practical applications. The results of ultimate elongation are given in Table 2. The regression equation for the ultimate elongation of these WPU films is of the following form:

$$\epsilon = 24.72x_2 + 28.22x_3 + 183.82x_1x_2 + 136.15x_2x_3 + 187.17x_1x_3 \quad (7)$$

(16.7) (16.7) (61.4) (73.7) (61.4)

The value of R^2_{adj} (= 0.87) indicates that the regression model is statistically significant. The dependence of the ultimate elongation of WPU films on the composition of the IPDI–H_6XDI–XDI ternary isocyanate system is shown in Fig. 11. Maximum elongation (*ca*. 70%) occurs in IPDI–H_6XDI–XDI ternary mixed systems possessing about 1/3 content of each diisocyanate component. The mixing of ternary diisocyanates effectively increases the ultimate elongation of polymer films because of the increase of mesophasic randomness in WPU polymer chains.

3.7. Wide-angle X-ray diffraction

Fig. 12 shows a comparison of the X-ray diffraction patterns of (1) PBA polyol, (2) IPDI-based WPU, (3)

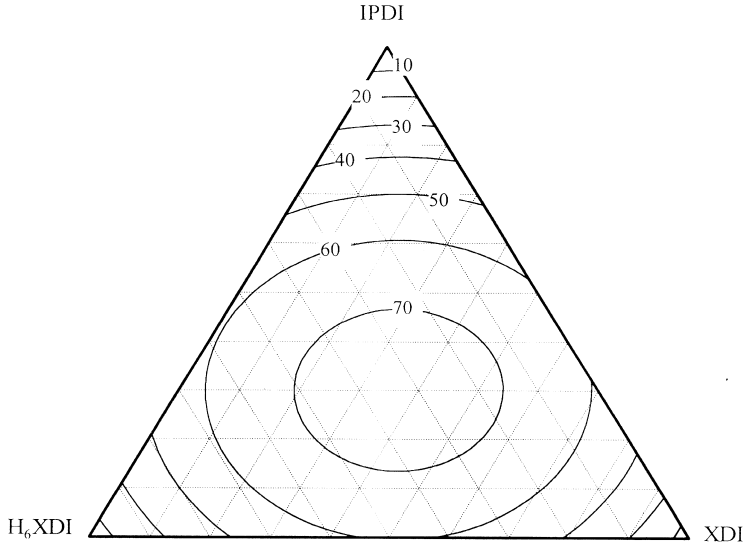

Fig. 11. Contour line plot of ultimate elongation (%) against diisocyanate compositions for IPDI–H_6XDI–XDI ternary diisocyanate-based WPU dispersions.

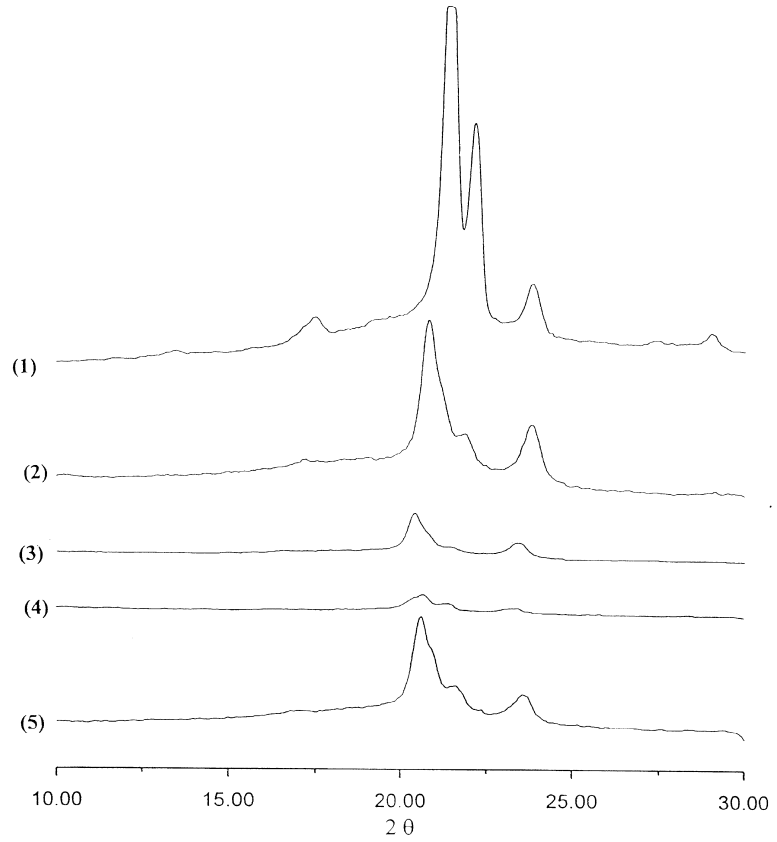

Fig. 12. Wide-angle X-ray diffraction patterns of PBA polyol and WPU films.

H_6XDI-based WPU, (4) XDI-based WPU, and (5) $\frac{1}{3}$IPDI/$\frac{1}{3}H_6$XDI/$\frac{1}{3}$XDI-mixed WPU samples, respectively. The PBA polyol exhibits five distinct diffraction peaks at $2\theta =$ 17.65, 20.70, 21.65, 23.80 and 28.75, respectively, for the (110), (113), (222), (200) and (213) planes. On the other hand, a small peak at $2\theta = 28.75$ in all of the WPU samples is virtually missing. Furthermore, the X-ray diffraction pattern of the IPDI-based WPU shows a peak at $2\theta = 20.7$ with a barely visible shoulder at $2\theta = 21.65$ on the corresponding halo of (311) plane, while the peak at $2\theta = 17.65$ decreases in comparison with that of the PBA polyol. This suggests that the crystallinity of IPDI-based WPU decreases as a result of IPDI-molecule incorporation in the PBA polymer chain. The X-ray diffraction pattern of the H_6XDI-based WPU shows only two peaks at $2\theta = 20.5$ and 23.7, respectively. The diffraction pattern of the XDI-based WPU is significantly different from those of both IPDI and H_6XDI-based WPU samples, however, the crystallinity level is relatively low. The X-ray diffraction pattern of the $\frac{1}{3}$IPDI/$\frac{1}{3}H_6$XDI/$\frac{1}{3}$ XDI-mixed WPU shows all four diffraction peaks similar to the IPDI-based WPU. However, the intensity of the diffraction peaks of the $\frac{1}{3}$IPDI/$\frac{1}{3}H_6$XDI/$\frac{1}{3}$XDI-mixed WPU is smaller than that of the IPDI-based WPU, indicating a lower crystallinity in the former. Direct polarized microscopy observation of the crystalline morphology of these samples will be discussed in the following section.

3.8. Polarized microscopy observation

To observe the changing trends, polarized microscopy (POM) was performed on a series of WPU samples which were cast on solid glasses and dried at 30°C. Since they were all similar, only four representative results are discussed here. Fig. 13 shows the POM for the WPU samples. An examination of Fig. 13 reveals that typical spherulitic structure of the order of several micrometers is visible. The spherulites are embedded in the anisotropic matrix. Note in Fig. 13*a–d* that the spherulitic size of XDI-based WPU is always the largest (Fig. 13*c*), and the IPDI or H_6XDI-based WPU followed next (Fig. 13*a, b*), with the ternary diisocyanate-mixed WPU being the smallest (Fig. 13*d*). Thus, in most cases the spherulites are of hard segment nature [40]. It must be noticed that no distinct Maltese cross in smaller spherulites was observed in the $\frac{1}{3}$/IPDI/$\frac{1}{3}H_6$XDI/$\frac{1}{3}$XDI-mixed WPU samples (Fig. 13*d*). This suggests that the fibrillar crystals are irregularly arranged in these spherulites.

4. Conclusions

By using statistical design strategy, the full compositional range of IPDI–H_6XDI–XDI ternary diisocyanate compositions was modelled with a limited number of experiments.

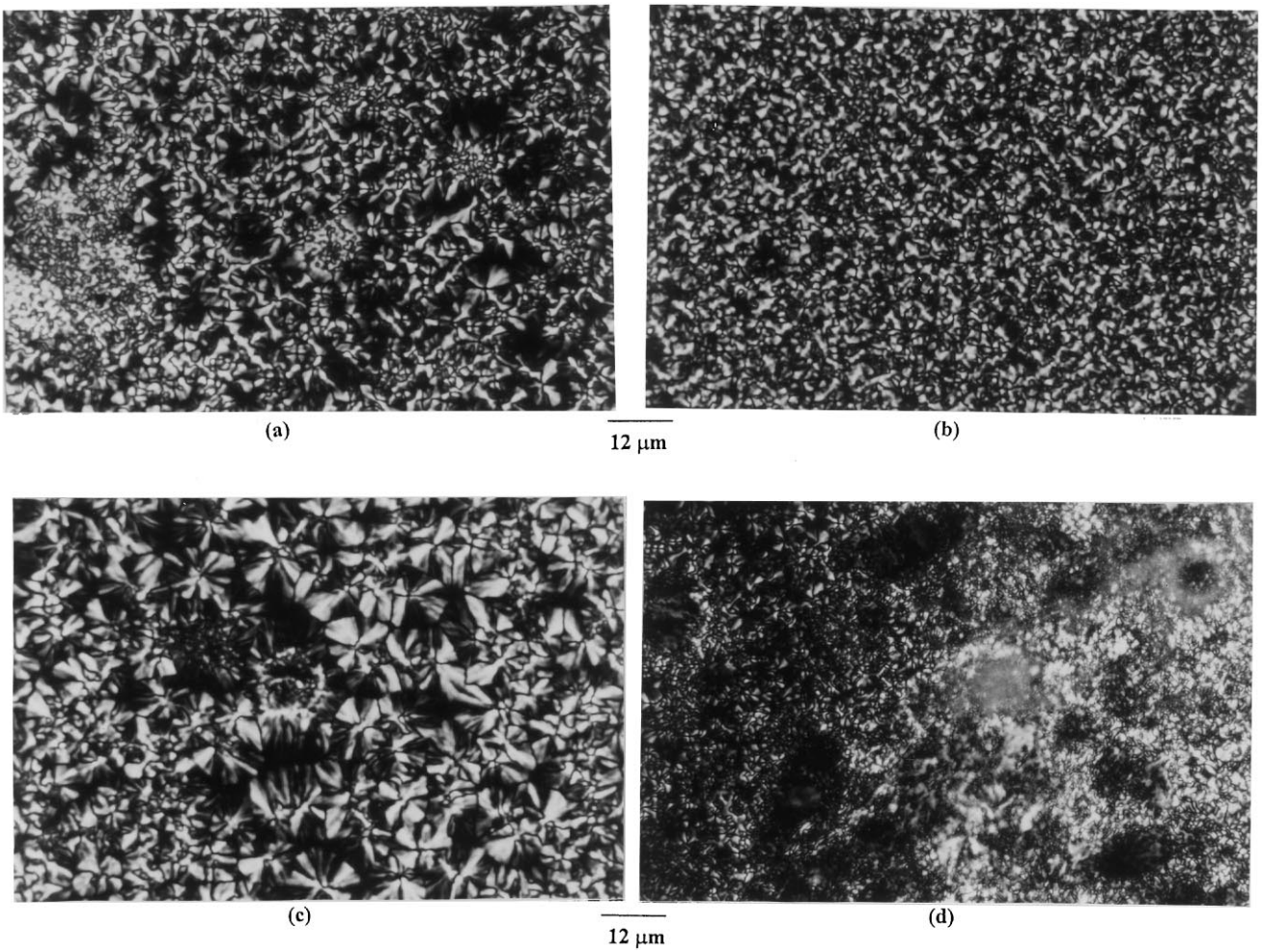

Fig. 13. Polarizing optical micrographs of WPU films. The samples are (a) pure IPDI-based WPU, (b) pure H_6XDI-based WPU, (c) pure XDI-based WPU and (d) $\frac{1}{3}$IPDI/$\frac{1}{3}$$H_6$XDI/$\frac{1}{3}$XDI-mixed WPU dispersions, respectively.

The coefficients of the regression models, represented as contour plots, were extremely useful in studying the effects of diisocyanate composition on the corresponding properties ($\nu, D_p, T_m^L, T_m^U, \gamma, \tau, \epsilon$). The ν results showed that the solution viscosity of H_6XDI–XDI binary WPU dispersions is the highest. Maximum particle sizes were demonstrated in the IPDI–XDI binary system possessing 45–90% IPDI content. The film of pure IPDI-based WPU demonstrated the highest tensile strength; while the longest ultimate elongation occurred in IPDI–H_6XDI–XDI ternary systems with 33% diisocyanate content. It is important to note that PBA polyol and its converted WPU exhibit doublet melting behaviour from DSC results. A plot of $1/T_m^L$ against $-\ln X_{IPDI}$ is approximately linear, indicating that the hard segments are randomly distributed along the molecular chain of the WPU. These WPU films demonstrated the existence of spherulite structure from the examination of polarized microscopy.

Acknowledgements

The financial support of this work by the National Science Council of the Republic of China under contract no. NSC87-2214-E-006-026 and NSC 87-2218-E-168-006 is gratefully acknowledged.

References

[1] Takahashi T, Hayashi N, Hayashi S. J Appl Polym Sci 1996;60:1061.
[2] Lorenz R, Els M, Haulena F, Schmitz A, Lorenz O. Angew Makromol Chem 1990;180:51.
[3] Earnst TR, Macknight WJ. J Polym Sci, Part D: Macromol Rev 1981;16:41.
[4] Dieterich D. Prog Org Coat 1981;9:281.
[5] Tirpak RE, Markusch PH. J Coat Technol 1986;58:49.
[6] Tembaum A, Rile H, Somoano RV. J Polym Sci, Part B: Polym Lett 1970;8:457.
[7] Al-Salah HA, Xiao HX, Malean JA, Frisch KC. J Polym Sci, Part A: PolymChem 1988;26:1609.
[8] Chen SA, Chan WC. J Polym Sci Part B: Polym Phys 1990;28:1499.
[9] Chan WC, Chen SA. Polymer 1995;1988:29.
[10] Al-Salah HA, Frisch KC, Xiao HX, Malean JA. J Polym Sci, Part A: PolymChem 1987;25:2127.
[11] Lorenz O, Hick H. Die Angew Makromol Chem 1978;72:115.
[12] Miller JA, Jwang KKS, Cooper SL. J Macromol Sci, Phys 1993;B22:321.
[13] Kim BK, Lee YM. Colloid Polym Sci 1992;270:956.
[14] Rahan H, Rahalingam P, Radhakrishnan G. Polym Commun 1991;32:93.

[15] Hwang KKS, Yang CZ, Cooper SL. Polym Engng Sci 1981;2:1027.
[16] Chen Y, Chen YL. J Appl Polym Sci 1992;46:435.
[17] Xu HS, Yang CZ. J Polym Sci Part B: Polym Phys 1995;33:745.
[18] Eisenberg A, King M. *Ion Containing Polymers: Physical Properties and Structure*. Academic Press, New York, 1997.
[19] Mooney M. J Appl Phys 1940;11:582.
[20] Lee DC, Register RA, Yang CZ, Cooper SL. Macromolecules 1988;21:998.
[21] Yang CH, Lin SM, Wen TC. Polym Engng Sci 1995;35:722.
[22] Yang CH, Wen TC. Ind Engng Chem Res 1997;36:1614.
[23] Xu MX, Liu WG, Wang CL, Gao ZX, Yao KD. J Appl Polym Sci 1996;61:2225.
[24] Kim BK, Kim TK, Jeong JM. J Appl Polym Sci 1994;53:371.
[25] Cornell, JA, *Experiments with Mixtures: Design, Models and the Analysis of Mixture Data*, 2nd edn. John Wiley, New York, 1990.
[26] Draper NR, Smith H. in *Applied Regression Analysis*, 2nd edn. John Wiley, New York, 1981, pp. 294–379.
[27] Oertel G, in *Polyurethane Handbook*, Vol. 195. Hanser, New York, 1994, p. 27.
[28] Holdsworth P, Turner-Jones A. Polymer 1971;12:195.
[29] Alfonso GC, Pedemonte E, Ponzetti L. Polymer 1979;26:104.
[30] Lin SB, Koenig JL. J Polym Sci, Polym. Phys. Ed. 1983;21:2365.
[31] Fountain F., Ledent J., Groeninckx G., Reynaers H. Polymer 1982;23:185.
[32] Hobbs S. Y., Pratt C. F. Polymer 1975;16:462.
[33] Stein R. S., Misra A. J Polym Sci, Polym. Phys. Ed. 1980;18:32.
[34] Yeh J. T., Runt J. J Polym Sci, Polym. Phys. Ed. 1989;27:1543.
[35] Ludwig H. J., Eyerer P. Polym. Engng Sci. 1988;28:143.
[36] Woo E. M., Chen J. M. J Polym Sci, Polym Phys 1985;1995:33.
[37] Woo EM, Ko TY. Colloid Polym Sci 1996;274:309.
[38] Flory PJ. Trans Faraday Soc 1955;51:848.
[39] Thomos EL, Reffner JR, Bellare J, in *International Workshop on Geometry and Interface*, September 1990, pp. C7–363.
[40] Janik H, Foks J. Cellular Polymers 1992;11:4.